Journal of
Marine Science and Engineering

MDPI

Article

Numerical Study of Nonlinear Effects on the Performance of the Self-Protected Energy Concentrator

Hangwei Zhang [1,2], Ting Cui [1] and Guanghua He [1,2,*]

[1] School of Ocean Engineering, Harbin Institute of Technology, Weihai 264209, China; jupi222319@163.com (H.Z.); cuiting_heu@hotmail.com (T.C.)
[2] Shandong Institute of Shipbuilding Technology, Weihai 264209, China
* Correspondence: ghhe@hitwh.edu.cn

Abstract: Wave concentrators have important application value in ocean engineering. Moreover, the performance of a concentrator on structural protection is important in the context of the complex ocean environment. A series of numerical simulations of the self-protected energy concentrator (SPEC) is performed under nonlinear wave conditions. The SPEC includes eight truncated cylinders arranged in a concentric circle. The performance of SPEC and the distribution of fluid field are studied by establishing a computational fluid dynamics (CFDs) model. It can be concluded that increasing wave steepness can weaken the self-protection performance and concentration effects due to its strong nonlinearity. The wave directions have little effect on the performance of SPEC. In addition, the change based on the target wave number can result in poor performance of SPEC.

Keywords: nonlinear waves; energy concentration; self-protection; CFD

check for updates

Citation: Zhang, H.; Cui, T.; He, G. Numerical Study of Nonlinear Effects on the Performance of the Self-Protected Energy Concentrator. *J. Mar. Sci. Eng.* **2023**, *11*, 2241. https://doi.org/10.3390/jmse11122241

Academic Editor: Eugen Rusu

Received: 4 November 2023
Revised: 25 November 2023
Accepted: 25 November 2023
Published: 27 November 2023

1. Introduction

Wave energy plays a significant part in renewable energy areas due to the advantage of the effective production and net-zero environmental protection characteristics [1,2]. The wave energy density can be significantly increased in a specific area through the wave concentration, which is beneficial for improving the power of wave energy generation and reducing costs. Energy concentration has been widely and commercially used in solar energy harvesting, radio wave transmission and other technologies. Different wave energy generation methods based on the energy concentration have been proposed to solve the commercial application of wave energy, becoming a research hotspot over the past few years.

The lens based on wave refraction is a typical energy-concentration device. The forms of lenses include underwater submerged plates [3–5], multiple horizontal submerged cylinders [6,7], etc. In addition, Kim et al. [8] have applied metamaterials with microscale architectures to underwater lenses and proposed a gradient refractive index lens composed of micro-lattices.

Curved reflectors [9–11] mainly in parabolic shape realize wave energy concentration based on wave reflection. Mayon et al. [12] designed a wave energy capture device consisting of a parabolic reflector and a cylindrical oscillating water column (OWC), and the research results indicated that the wave energy capture of the device significantly increased due to the energy concentration of the reflector.

The concentrators introduced above make full use of wave characteristics including refraction and reflection, and effectively improve the wave energy generation power, but its protection problem has not been further studied. In the complex and changeable wave environment, improving the protection performance of the concentrator is conducive to reducing the costs and promoting engineering research on wave energy generation.

In the field of electromagnetic wave and sound wave, researchers [13–15] introduced the cloaking phenomenon and designed the material properties and size parameters of the structure to eliminate scattered waves. In recent years, the cloaking phenomenon has been applied to ocean engineering to reduce the impact of wave loads on structures. Porter [16] first introduced scattering cancellation method (SCM) to the wave field. Afterwards, Newman [17,18] extended the cloaking phenomenon to deep water regions and proposed two types of cloaking devices, the outer cylindrical array and the outer circular ring. Zhang et al. [19,20] proposed a self-protected energy concentrator (SPEC) with cylindrical array structure based on SCM. The performance of the SPEC has been experimentally and numerically studied, and its effectiveness has been proved, especially under linear wave conditions. However, the performance of the SPEC under nonlinear waves remains to be studied.

Potential flow theory [21–24] is a classic numerical method for solving the interaction between waves and cylindrical structures. However, the potential flow theory ignores the viscous effect of incompressible fluid, which may influence the accuracy of the numerical calculation results. Lu et al. [25] calculated the resonant wave height between two close bodies and compared the numerical results of computational fluid dynamics (CFDs) and potential flow theory. The results showed that CFDs can predict wave height more accurately, and the problem of inaccurate prediction of potential flow theory can be solved by introducing artificial viscous dissipation coefficient. Sun et al. [26] calculated the wave force on a single cylinder and the free surface height surrounding the cylinder through the CFD solver OpenFOAM and the potential flow solver DIFFRACT, respectively. By comparison, it can be found that CFD can provide more accurate prediction results at large wave steepness due to its ability to simulate components beyond the second harmonic.

In recent years, CFD method has been widely applied to solve the complex interaction between the cylindrical structures and nonlinear waves, taking into account the influence of liquid viscous effects. Mohseni et al. [27] conducted the investigation to investigate wave run-up on a fixed cylinder at different wave steepness, and the comparison between experiment data and numerical results showed that CFD has the ability to accurately simulate nonlinear wave interaction with coastal structures. A range of numerical simulations were conducted by Chen et al. [28] to study the wave run-up of four cylinders, and a good agreement was observed between numerical results and experiment data under several designed wave steepness. Wang et al. [29] used OpenFOAM to numerically study the interaction between a heaving cylinder and waves, and the results showed that the maximum run-up altitude around the heaving cylinder varies nonlinearly due to the changes in wave frequency, and the wave force increases nonlinearly with the increased wave numbers.

In this paper, the SPEC designed by Zhang et al. [20] is taken as the research objective, and the commercial CFD solver STAR-CCM+ is employed to study the self-protection performance and concentration effects under nonlinear waves. The research contents are structured as follows: In Section 2, the numerical theory and the numerical model are presented. In Section 3, the verification of the model is described. Section 4 presents the performance of the SPEC against different conditions, including different wave steepness, wave directions and wave numbers. Finally, the main conclusions are given in Section 5.

2. Theory Models

The numerical simulations are conducted by using the commercial CFD solver STAR-CCM+. In this section, the theory models are described including turbulence model, governing equations and interface capturing.

2.1. Governing Equations

In this study, the commercial CFD solver STAR-CCM+ is applied to solve Reynolds-averaged Navier–Stokes (RANS) equations for the flow of air and water, the 3D continuity equation and momentum equation are shown as Equations (1) and (2), respectively. Based on the incompressible fluid assumption, finite volume method and second-order time discretization are used to solve the three-dimensional unsteady motion of waves. Realizable k-ε model [30] is applied for turbulence modeling in this study.

$$\frac{\partial \overline{u}_i}{\partial x_i} = 0 \tag{1}$$

$$\frac{\partial \overline{u}_i}{\partial t} + \overline{u}_j \frac{\partial \overline{u}_i}{\partial x_j} = -\frac{1}{\rho}\frac{\partial \overline{p}_i}{\partial x_i} + \frac{\partial}{\partial x_i}[(\nu + \nu_t)(\frac{\partial \overline{u}_i}{\partial x_i} + \frac{\partial \overline{u}_j}{\partial x_j})] + g_i \tag{2}$$

where $\overline{u}_i$, p_i, ρ, ν and ν_t represent the time-average velocity, pressure, fluid density, kinematic viscosity and eddy viscosity, respectively.

2.2. Interface Capturing

The free surface is determined with the volume of fluid (VOF) method. In this way, the volume fraction $\alpha \in [0, 1]$ represents the amount of fluid in each cell.

$$\alpha(x,t) = \begin{cases} 1, & \text{water} \\ 0 < \alpha < 1, & \text{interface} \\ 0, & \text{air} \end{cases} \tag{3}$$

Based on the value of α, the fluid properties can be calculated in each cell, such as density ρ and kinematic viscosity ν.

$$\rho = \alpha\rho_{\text{water}} + (1-\alpha)\rho_{\text{air}} \tag{4}$$

$$\nu = \alpha\nu_{\text{water}} + (1-\alpha)\nu_{\text{air}} \tag{5}$$

3. Model Verification

The verification of numerical models is performed in this section, including the establishment of the numerical wave tank, the studies of mesh convergence and time-step convergence. In addition, a simulation of wave interaction with a fixed single cylinder is carried out to confirm the validity of the wave–object interaction model.

3.1. Numerical Wave Tank

As shown in Figure 1, the length of the numerical wave tank is $6L$ (L is the incident wavelength) and the width is $3L$. The left side of the NWT is the inlet boundary, and the right side is the outlet boundary. The flow direction can be specified in STAR-CCM+ to set the *VelocityInlet* as the outlet boundary. The left and right walls are the no-slip walls, and so is the bottom. The top boundary is free to the atmosphere, and the pressure outlet boundary is applied.

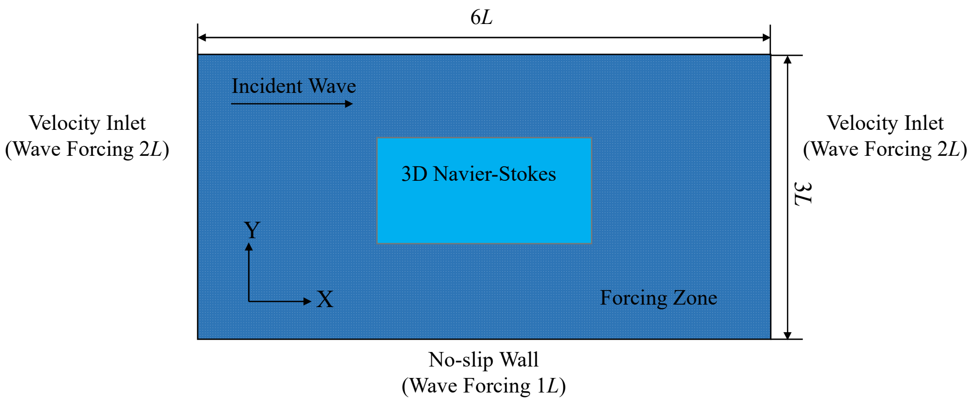

Figure 1. Numerical wave tank (top view).

As can be seen from Figure 1, wave forcing is applied in the Forcing zone (dark blue region), and the solution of 3D Navier–Stokes is conducted in the light blue region of the computation domain. The wave forcing matches a wave solution obtained by the CFD solution near the structure with the Euler equation solver at far field, and it decreases the computational time with a reduced-size solution domain [31]. Due to the damping properties of the gradual forcing, the wave forcing also eliminates problems related to surface wave reflection at boundaries [32]. The extruder mesh is used in x and y directions to save the computational time.

3.1.1. Mesh Convergence

Firstly, the mesh convergence of the numerical wave tank was studied comparing the wave elevation at different position along tank in this section. Three types of mesh are used in this study. The specific mesh sizes are shown in Table 1, η_0 is wave elevation, L is wave length. For all three meshes, the mesh size at free surface is 25% of the base size in the x direction and 6.25% of the base size in the z direction. The mesh distribution of the NWT is shown in Figure 2, and the yellow line represents still water surface. Two wave probes are arranged at $1L$ and $3L$ from the wave generating boundary, respectively.

Table 1. Meshes size.

Mesh	Base Size (m)	$L/\Delta x$	$\eta_0/\Delta z$
A	0.12	63	10
B	0.064	117	18
C	0.056	134	21

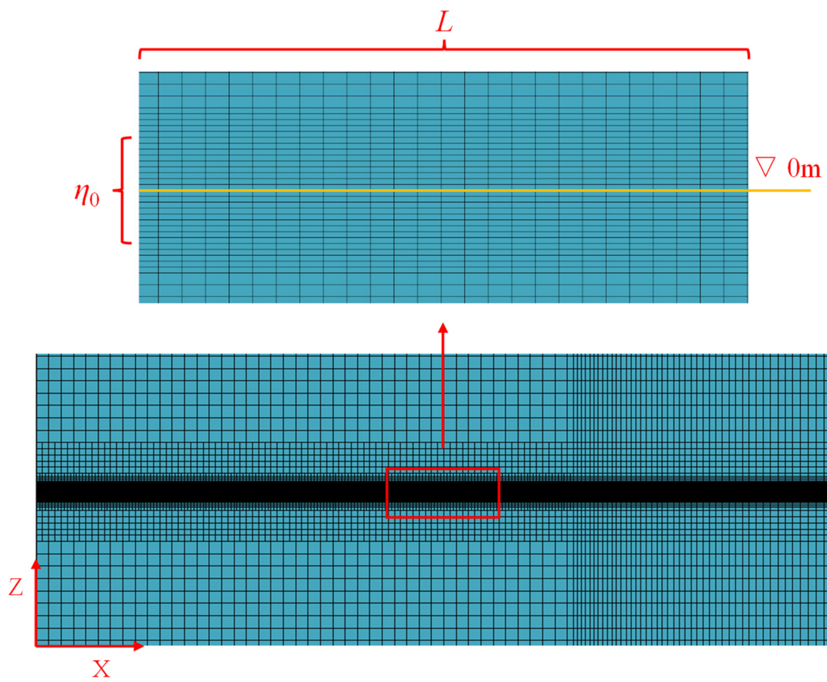

Figure 2. Mesh refinement.

The wave parameters used in this section are shown in Table 2, which are consistent with Zhang et al.'s experiment [20]. In Table 1, $S = \eta_0/L$ is wave steepness, η_0 is wave elevation, L is wave length, T is wave period.

Table 2. Wave parameters.

S	η_0 (m)	L (m)	T (s)
0.04	0.075	1.878	1.1

Figure 3 shows the wave elevations against various positions. It is clear that the wave elevations of three type of meshes are basically the same at $1L$ from the wave generating boundary, and the relative error between the incident wave elevation and the wave elevations at $3L$ from the wave generating boundary is 5.14%, 3.96%, 3.64%, respectively. Considering the accuracy of numerical values and calculation cost, the size of Mesh B is applied in the subsequent study.

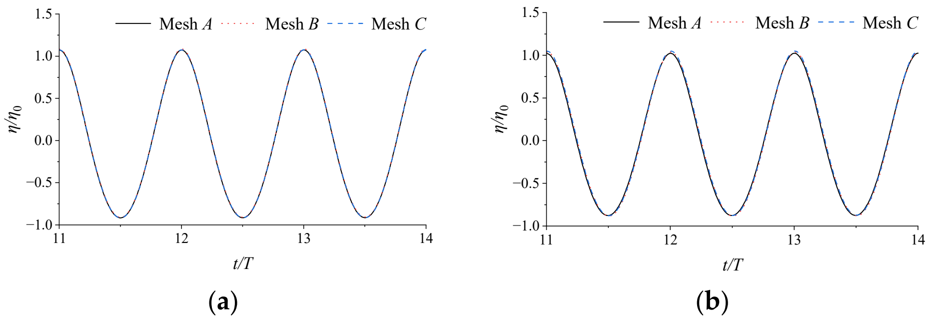

Figure 3. Time history of wave elevation at different positions (**a**) $1L$ from the wave generating boundary; (**b**) $3L$ from the wave generating boundary.

3.1.2. Time-Step Convergence

Under the same wave conditions shown in Table 2, time-step convergence of Mesh B was carried out. Based on the principle that the Courant number is less than 1 at free surface, $\Delta t = T/220$, $T/440$ and $T/660$ are set as time steps, respectively, T is wave period. Figure 4 presents the wave elevation at $3L$. It can be found that the wave elevation at $\Delta t = T/220$ is significantly lower than that at $\Delta t = T/440$ and $\Delta t = T/660$, and the wave elevations of $\Delta t = T/440$ and $\Delta t = T/660$ are basically the same. To balance the accuracy of numerical values and computational cost, $\Delta t = T/440$ is adopted in the subsequent calculations.

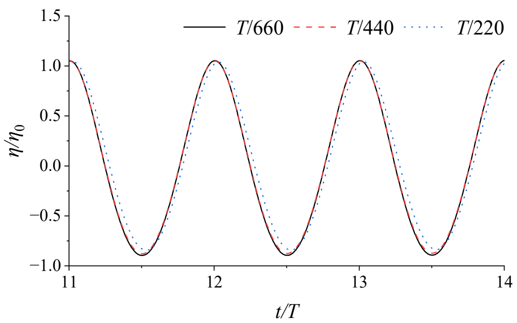

Figure 4. Time history of wave elevation at $3L$ from the wave generating boundary under different time steps.

3.2. *Validation of the Numerical Model*

The validity of the numerical model was proved by the comparison of the numerical values with experimental data from Mo et al. [33]. Figure 5a shows the settings of numerical model. The origin of the coordinates of the simulation domain is located at the center of the structure, with $z = 0$ located at the still water level. The negative x-axis is the direction of the incident wave. As the structure is an axial symmetrical distribution in x-z plane, we use half of the computational domain to reduce the calculation time. The single cylinder with a diameter of 0.35 m is fixed at the bottom of the wave tank. The water depth is 4.76 m. Table 3 presents the parameters of the incident wave. The arrangement of wave probes is plotted in Figure 5b. The specific positions of wave probes are depicted in Table 4, which refers to the experiment to illustrate the validity of the numerical model for wave–object interaction.

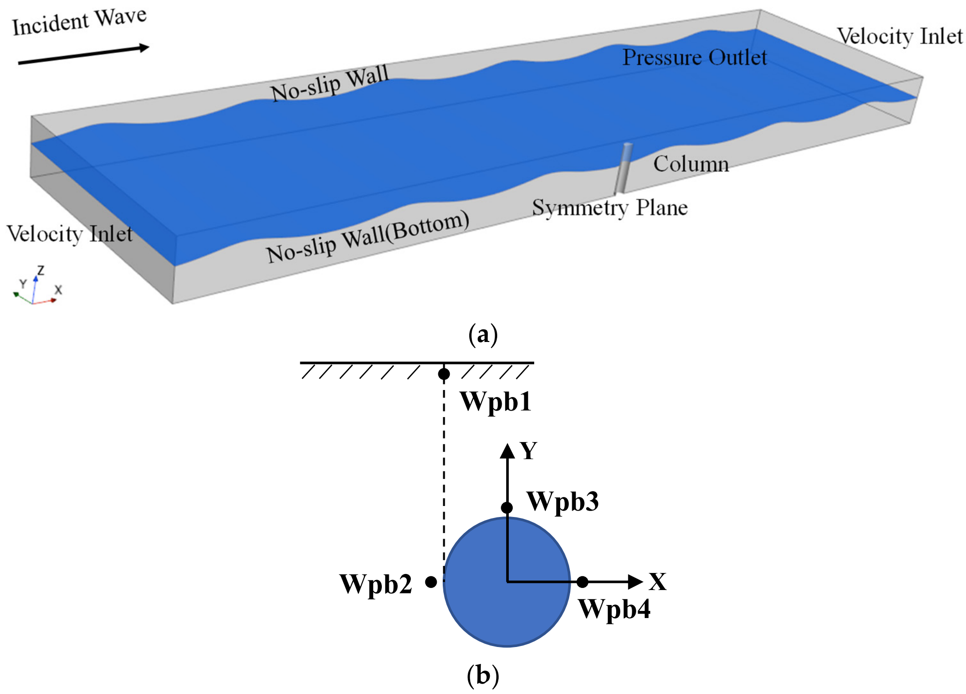

Figure 5. Numerical setup: (**a**) numerical wave tank; (**b**) arrangement of wave probes.

Table 3. Wave parameters to validate the model.

S	η_0 (m)	L (m)	T (s)
0.055	1.2	21.9	4

Table 4. Positions of wave probes set in wave tank.

Wave Probes	x (m)	y (m)
Wpb1	−0.35	32.75
Wpb2	−0.45	0
Wpb3	0	0.45
Wpb4	0.45	0

The numerical wave force on the cylinder is compared with the experimental results from Mo et al. [33], and a good agreement can be found in Figure 6.

In addition, Figure 7 shows the time history of wave elevations at different wave probes, where $\eta_{1,\max}$ represents the maximum wave elevation in wave probes Wpb1. It is obvious that the numerical data agree well with the experimental results, which shows that the wave–object interaction can be accurately simulated by the numerical model.

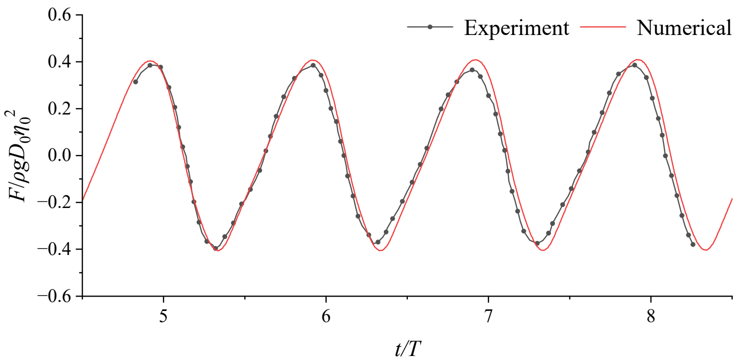

Figure 6. The experimental and numerical results of wave force.

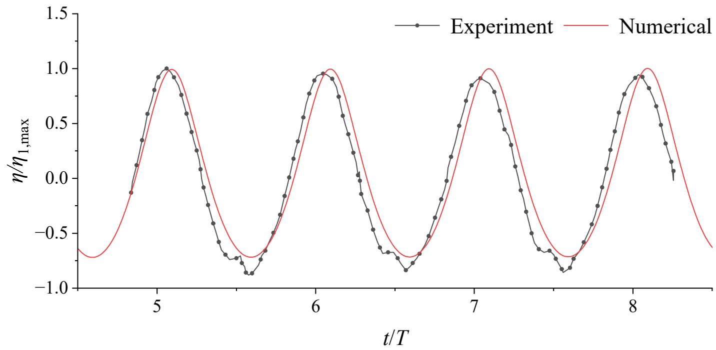

(**a**)

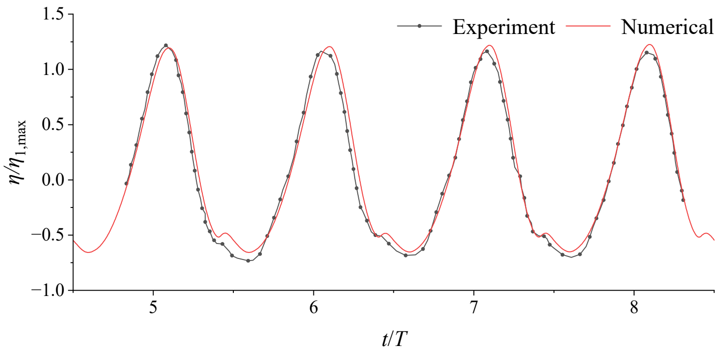

(**b**)

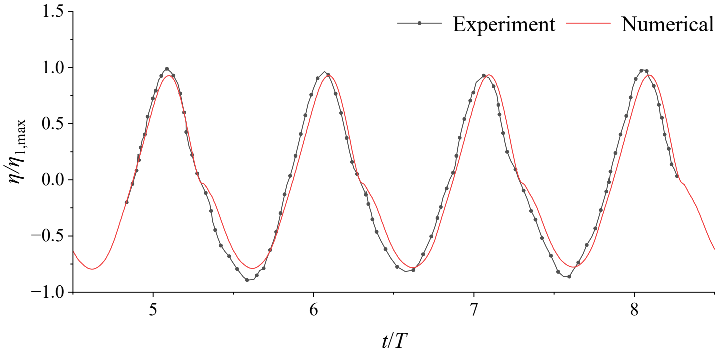

(**c**)

Figure 7. *Cont*.

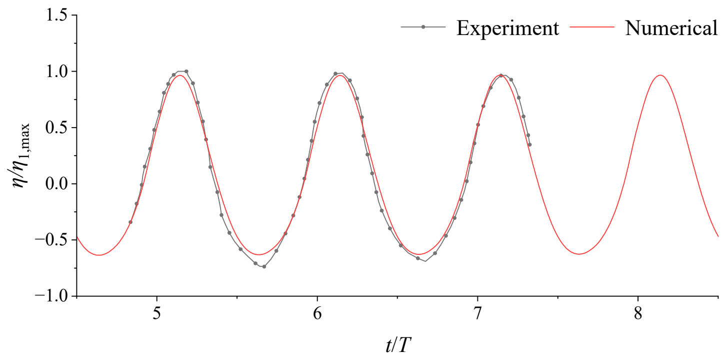

(**d**)

Figure 7. The experimental and numerical wave elevations at different wave probes: (**a**) Wpb1; (**b**) Wpb2; (**c**) Wpb3; (**d**) Wpb4.

4. Numerical Results

The self-protected energy concentrator (SPEC) [20] is a multi-cylinder array structure. To study the self-protection performance and concentration effects of the structure under nonlinear wave conditions, a series of numerical simulations were conducted based on the established numerical wave tank. The influence of viscous effects, wave steepness, wave direction and wave numbers are considered.

4.1. Viscous Effects on the SPEC

The numerical physical setting shown in Figure 8 includes eight identical truncated cylinders, which are arranged regularly in the form of concentric circles of radius R. The radius of the truncated cylinder is r = 0.125 m, the draft is d = 0.181 m, the length between the center of the array structure and the center of the small cylinder is R = 0.353 m and the water depth is 1.5 m.

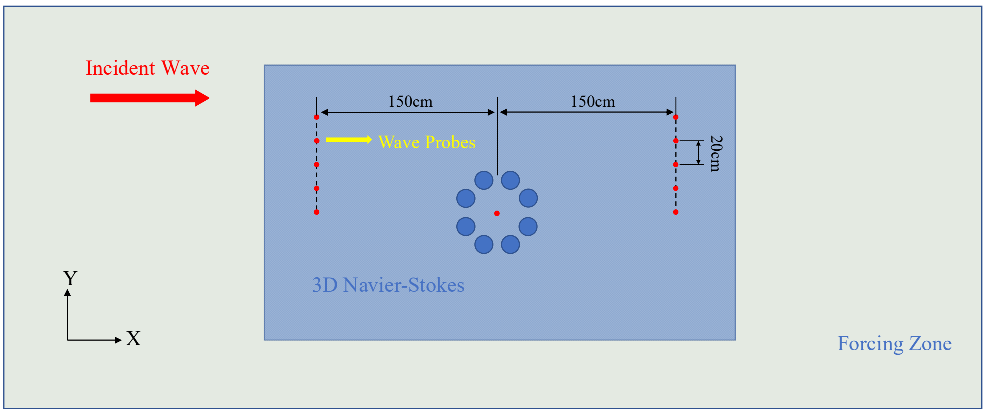

Figure 8. Schematic diagram of the SPEC.

As shown in Figure 8, 5 wave probes are arranged on the weather-side line and lee-side line that parallel to y-axis, respectively, 10 wave probes in all. Each line is 1.5 m away from the center of the structure, and the distance between adjacent wave probes on each line is 20 cm. In addition, a wave probe is set at the center of the structure. The origin of the coordinates is located in the center of the structure, with z = 0 located at the still water surface, and the incident wave is generating and propagating from the left side to right direction along x-axis. The method of forcing is applied to eliminate the wave reflection at boundaries.

The hydrodynamic characteristics of the SPEC at different wave steepness conditions were investigated to analyze the nonlinear wave effect. The wave parameters are shown in Table 5, and three wave-steepness conditions in a sequency of $S = 0.01$, $S = 0.02$ and $S = 0.04$ are considered.

Table 5. Wave parameters to investigate viscous effect.

S	η_0 (m)	L (m)	T (s)
0.01	0.019		
0.02	0.038	1.878	1.1
0.04	0.075		

Figures 9–11 show the numerical wave elevations at two outside lines under three wave-steepness conditions, and numerical results are compared with the potential flow values and experimental data [20]. It can be found that on the weather side, the results of CFD are in better agreement with the experimental data than the potential flow values, which indicates the importance of viscous effect in simulating the wave interaction with objects. On the lee side, the CFD calculation results are smaller than the experimental data, which may be due to the influence of numerical dissipation.

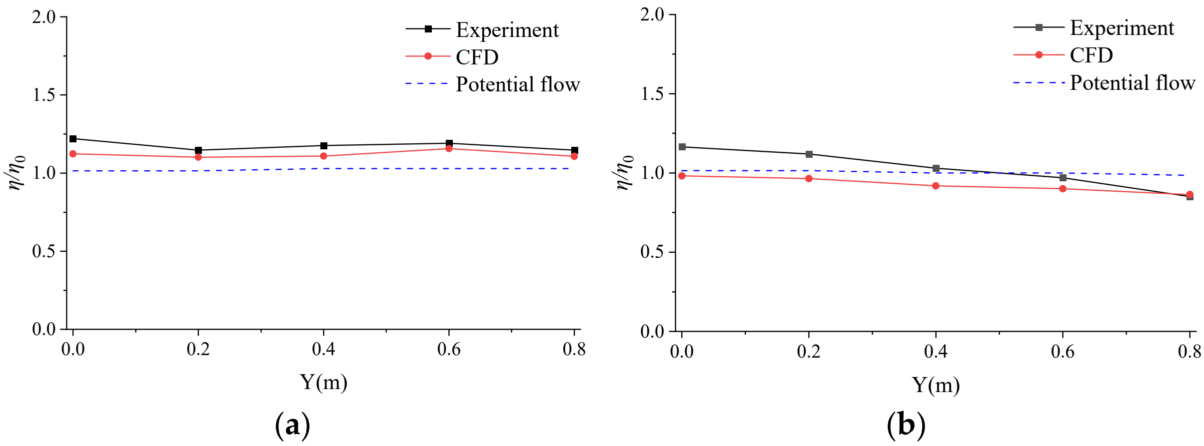

Figure 9. The comparison of wave heights at $S = 0.01$: (**a**) Weather side; (**b**) Lee side.

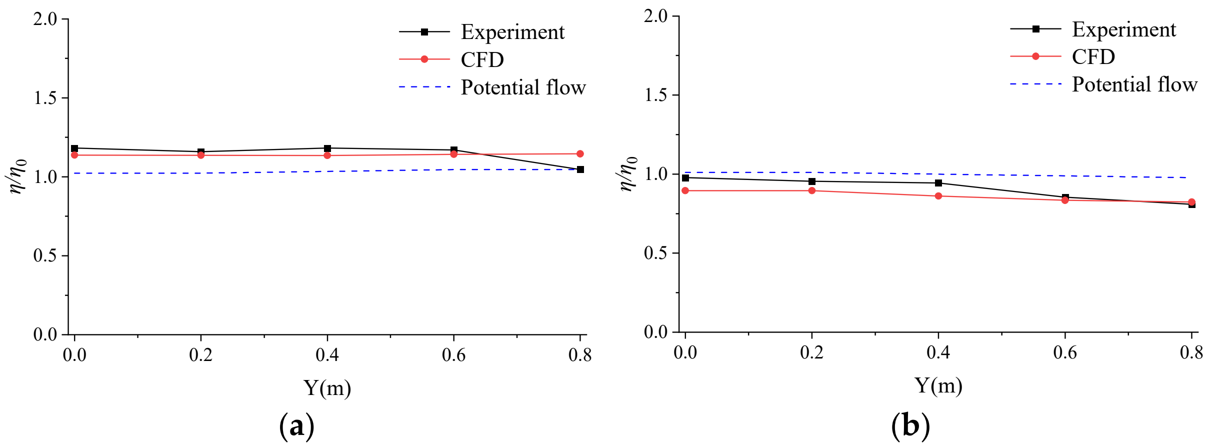

Figure 10. The comparison of wave heights at $S = 0.02$: (**a**) Weather side; (**b**) Lee side.

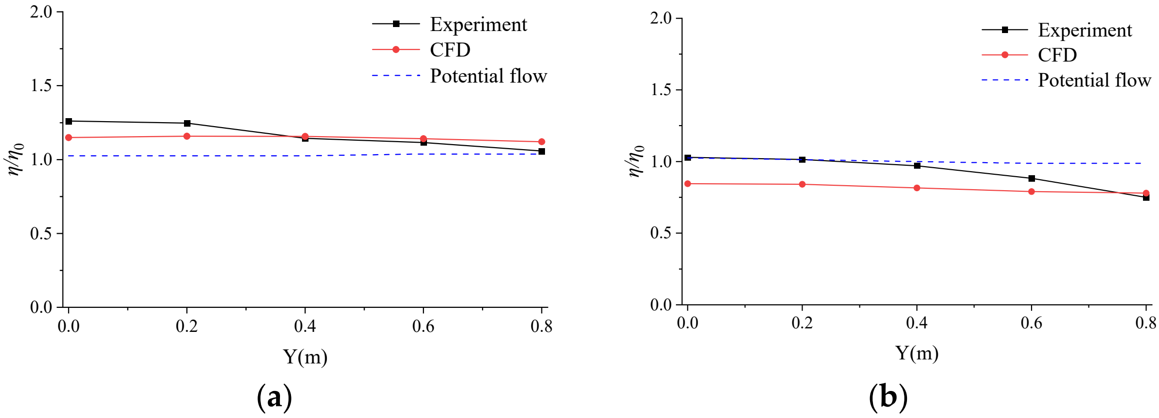

Figure 11. The comparison of wave heights at S = 0.04: (**a**) Weather side; (**b**) Lee side.

Figure 12 presents the dimensionless wave elevation η/η_0 at the central point. For different wave probes, average wave elevation of five wave periods is chosen as the numerical value. The wave elevation calculated by the potential flow theory keeps three times larger than the incident wave elevation. The nonlinear effect of waves enhances with increased wave steepness. The comparison between numerical values and experimental data shows that CFD can simulate the interaction between the SPEC and strong nonlinear waves more accurately.

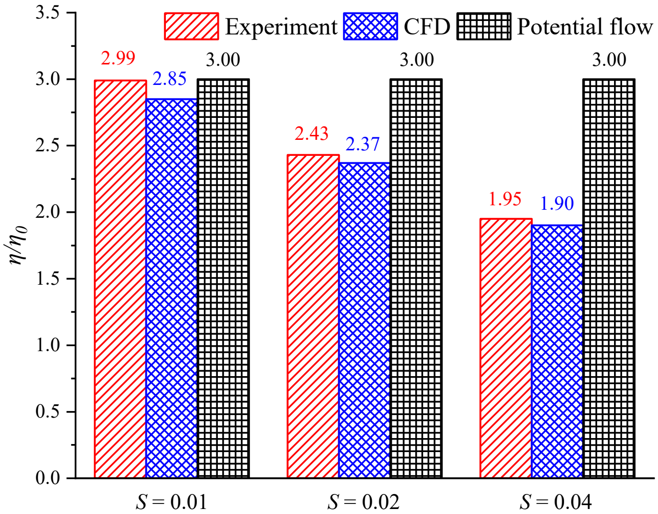

Figure 12. Dimensionless wave elevation (η/η_0) at the center of the SPEC.

4.2. Performance of the SPEC at Different Wave-Steepness Conditions

To study the effect of wave steepness on the properties of the SPEC, the wave distributions at four kinds of wave-steepness conditions (S = 0.02, S = 0.04, S = 0.06, S = 0.08) were numerically simulated. The wave conditions are presented in Table 6. The calculation results of S = 0.02 case and S = 0.04 case are consistent with those in Section 4.1, and are given here again for comparison.

Table 6. Wave parameters at different wave-steepness conditions.

S	η_0 (m)	L (m)	T (s)
0.02	0.038	1.878	1.1
0.04	0.075		
0.06	0.113		
0.08	0.15		

To better describe the self-protection performance of the SPEC, two single cylinders, namely big single-cylinder ($r_b = R + r = 0.478$ m) and small single-cylinder ($r_s = r = 0.125$ m), are considered for comparison, as shown in Figure 13. The drafts of two single-cylinders are the same as that of the SPEC. Figure 13a shows the number of each cylinder of the SPEC.

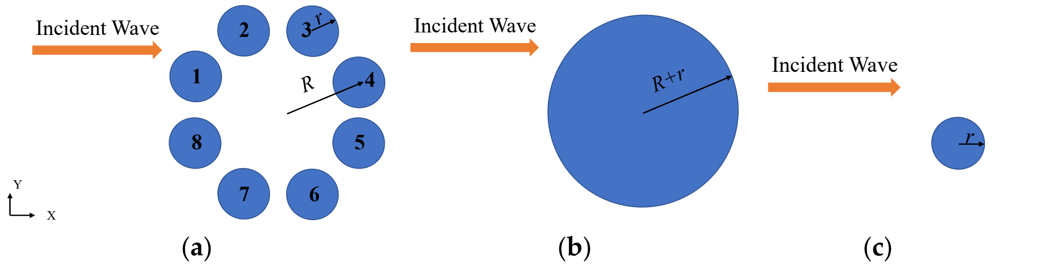

Figure 13. The diagram of structures: (**a**) the SPEC; (**b**) the big single-cylinder; (**c**) the small single-cylinder.

The influence of nonlinear waves on the self-protection performance was studied based on the wave elevations at ten probes outside the SPEC, including the two single cylinders shown in Figure 13a,b. From Figures 14–17, it can be seen that the results of the concentrator close to the values of the big single-cylinder gradually with the increase in wave steepness, which shows that nonlinear waves can weaken the self-protection performance of the SPEC.

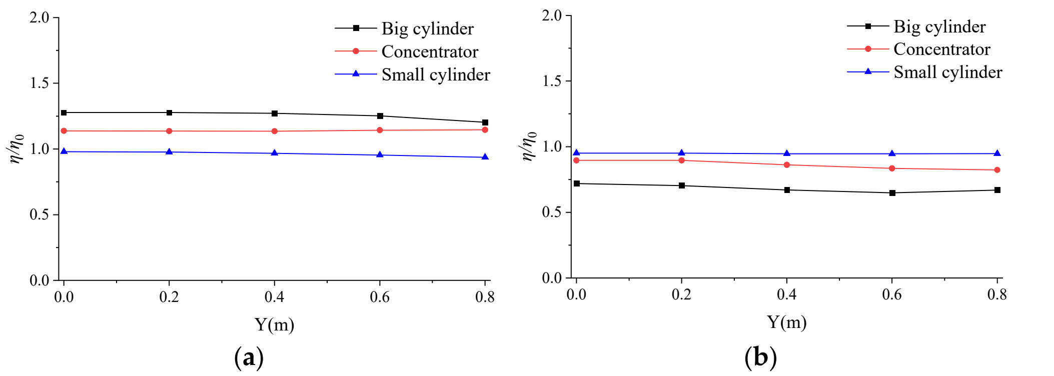

Figure 14. The numerical wave elevation at $S = 0.02$: (**a**) Weather side; (**b**) Lee side.

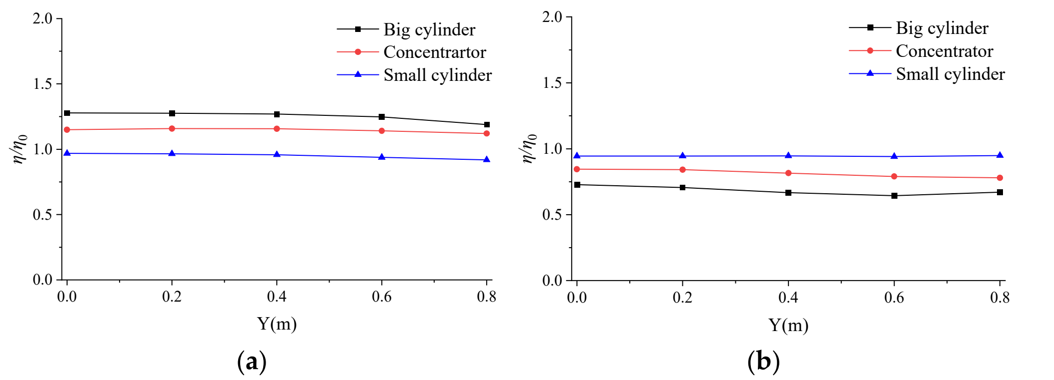

Figure 15. The numerical wave elevation at $S = 0.04$: (**a**) Weather side; (**b**) Lee side.

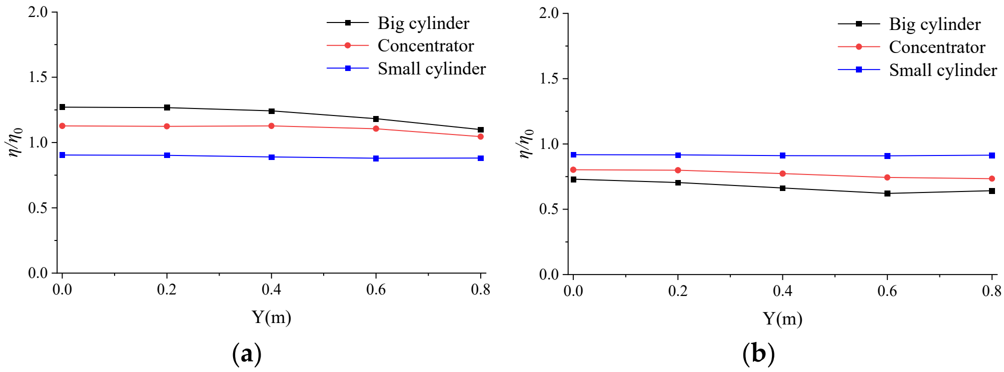

Figure 16. The numerical wave elevation at S = 0.06: (**a**) Weather side; (**b**) Lee side.

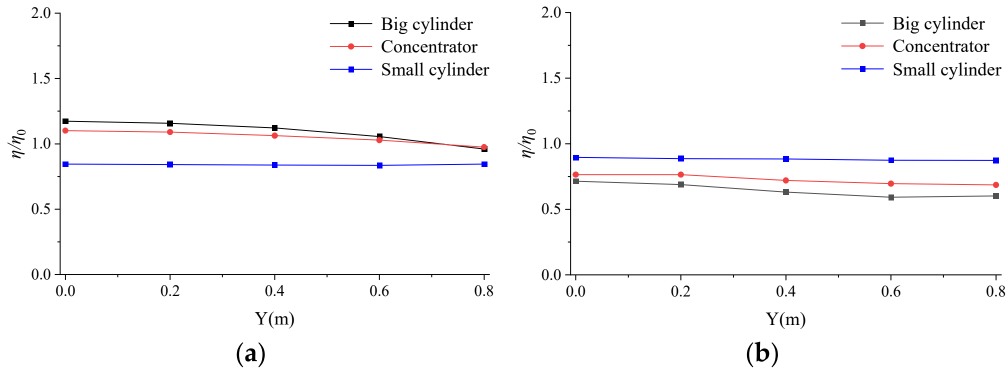

Figure 17. The numerical wave elevation at S = 0.08: (**a**) Weather side; (**b**) Lee side.

For wave steepness, the outer wave elevations of the small single-cylinder are close to the incident wave elevation, while the big single-cylinder has a large disturbance to the outer wave elevations. It is noted that the outer wave elevations of the SPEC are always between the numerical results of two single cylinders, which means that the SPEC still realizes self-protection under nonlinear waves to some extent.

Figure 18 compares the dimensionless wave elevation (η/η_0) of the center of the concentrator and gives partial experimental data. It can be seen that η/η_0 decreases gradually with the increase in wave steepness, indicating that nonlinear wave causes a negative impact on the concentration effects. However, it is noted that as the wave steepness reaches the maximum value S = 0.08, the η/η_0 is still greater than 1, indicating that the SPEC is still having effective performance of wave energy concentration under nonlinear waves.

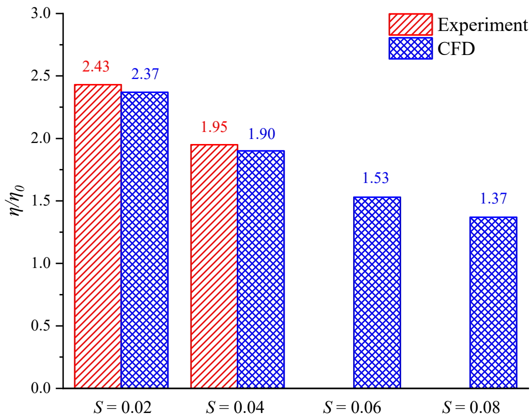

Figure 18. Dimensionless wave elevation (η/η_0) at the center of the SPEC under different wave-steepness conditions.

Figure 19 shows the wave profiles along the $y = 0$ section inside the concentrator to reveal the concentration effects at different wave-steepness conditions, while the numerical results correspond to the moment when the central wave probe monitors the maximum wave elevation. There are three regions after the division: region 1 ($x < -R$), region 2 ($-R < x < R$) and region 3 ($x > R$), and it is obvious that most of the wave power concentrates in region 2 ($-R < x < R$). At the same time, the nonlinear interaction between the waves and the SPEC enhances with increased wave steepness, resulting in the wave surface inside the concentrator no longer being symmetrical, about $x = 0$.

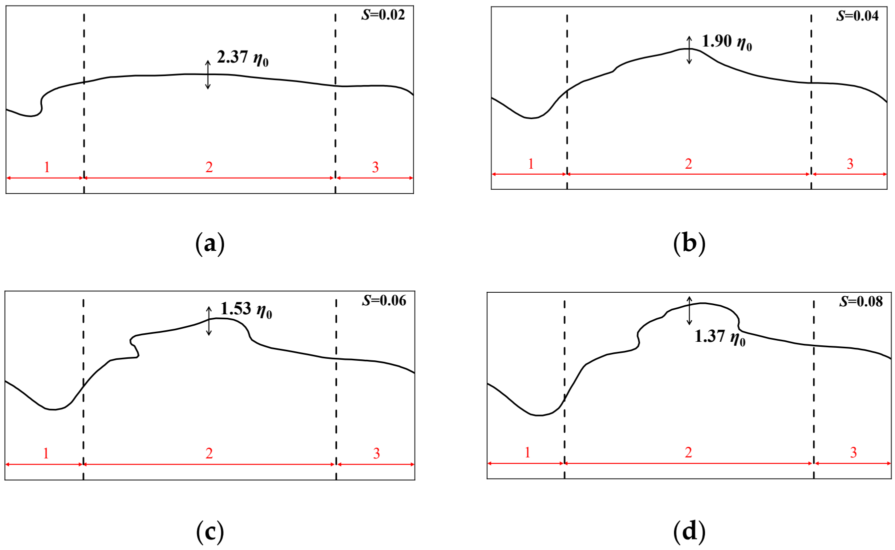

Figure 19. Wave profile along the $y = 0$ section inside the SPEC under four wave-steepness conditions: (**a**) $S = 0.02$; (**b**) $S = 0.04$; (**c**) $S = 0.06$; (**d**) $S = 0.08$.

With the comparison of the wave force on the SPEC and the small single-cylinder ($r_s = 0.125$ m), the protection problem is further studied. It can be observed from Figure 20 that the average wave forces on the SPEC are smaller than the values of a single small-cylinder under different wave steepness conditions, which implies that the concentrator has a good overall protection.

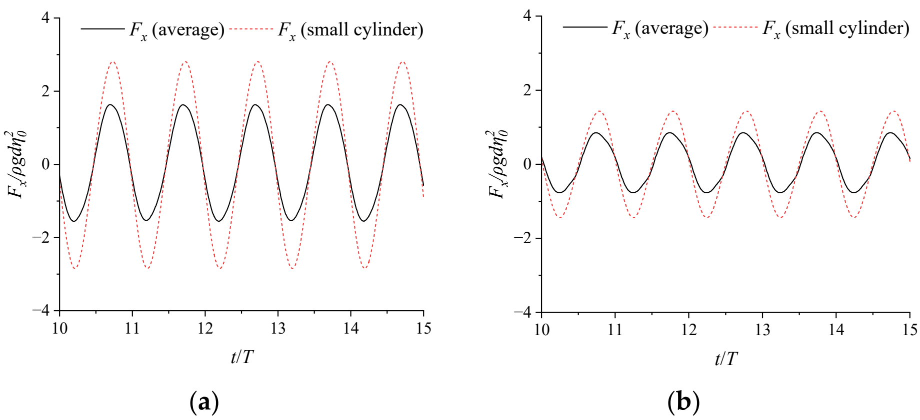

Figure 20. *Cont.*

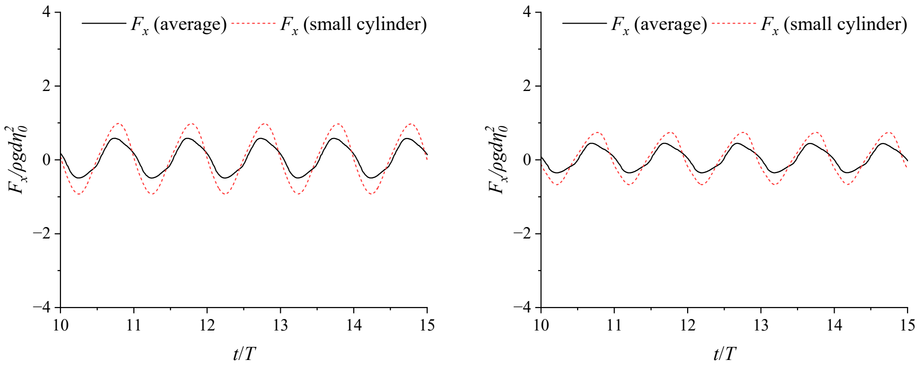

(**c**) (**d**)

Figure 20. Average wave forces on the SPEC at different wave-steepness conditions: (**a**) S = 0.02; (**b**) S = 0.04; (**c**) S = 0.06; (**d**) S = 0.08.

As shown in Figure 21, the wave forces of different cylinders are analyzed at S = 0.04. Since the concentrator is symmetrical at about y = 0, only the forces of cylinder 1, cylinder 2, cylinder 3 and cylinder 4 are simulated. It can be observed that the wave forces of cylinder 2–4 are close to that of the small single cylinder. In addition, it is noted that the interaction between waves and the SPEC results in strong nonlinearity of the wave force on cylinder 2. For the protection performance, each cylinder of the concentrator has better local protection except cylinder 1 and cylinder 8.

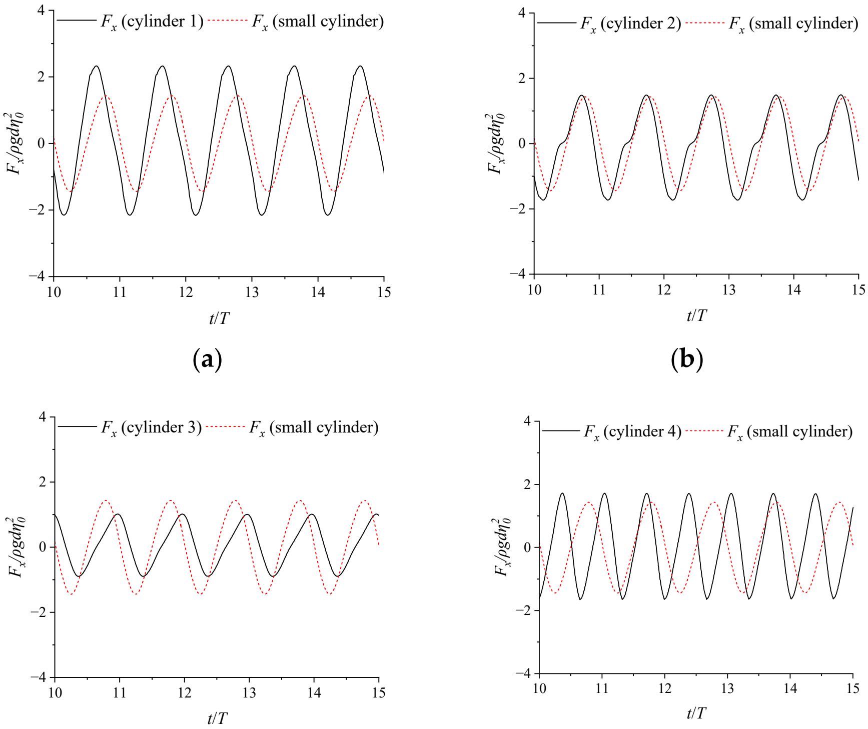

(**c**) (**d**)

Figure 21. Wave forces on the cylinders of the SPEC: (**a**) cylinder 1; (**b**) cylinder 2; (**c**) cylinder 3; (**d**) cylinder 4.

4.3. Performance of the SPEC at Different Wave Directions

The influence of different wave directions on the performance under nonlinear waves are discussed in this section. Due to the symmetry of the SPEC, only two wave headings are compared at S = 0.04, including 0° and 22.5°, as shown in Figure 22.

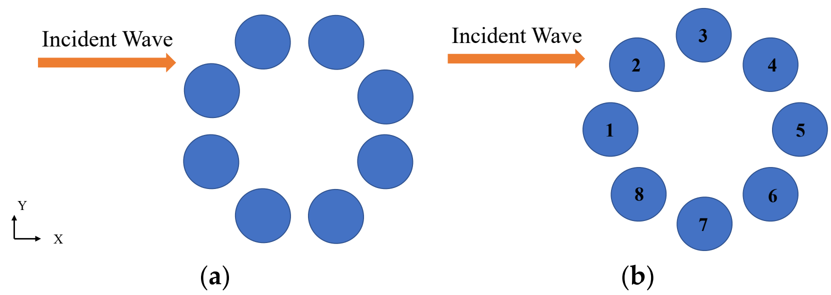

Figure 22. Schematic diagram of different wave directions: (**a**) heading 0°; (**b**) heading 22.5°.

From the numerical results shown in Figure 23, the wave elevations outside the concentrator are consistent, which indicates that the self-protection performance of the SPEC is not affected by the wave direction. In addition, Figure 24 shows that there is little difference in the concentration effects of the concentrator at different wave directions.

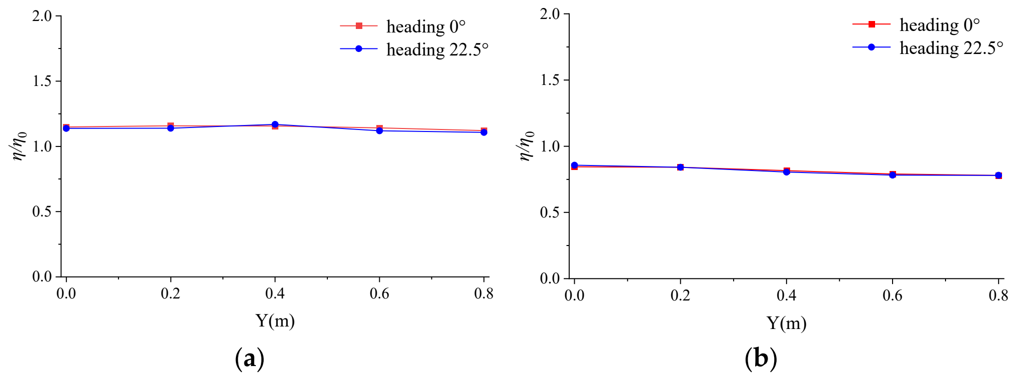

Figure 23. The wave direction effect on the self-protection performance at S = 0.04: (**a**) Weather side; (**b**) Lee side.

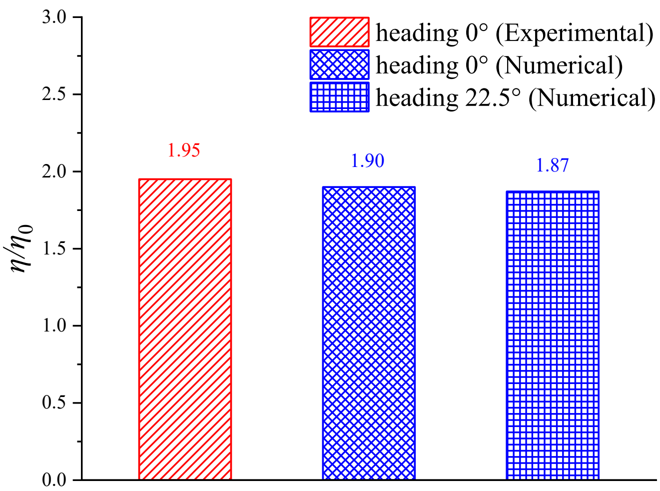

Figure 24. The wave direction effect on the concentration effects at S = 0.04.

The wave forces loading on the concentrator are plotted in Figure 25. Looking at the comparison in Figure 25a, the average wave force on the SPEC is smaller than that of the small single cylinder. The wave forces of cylinder 1, cylinder 2 and cylinder 5 within the concentrator system are greater than that of the small single cylinder. The wave force on cylinder 3 is minimal but the nonlinear effect is stronger due to the interplay between the surrounding cylinders and the waves. The local protection of the SPEC at heading 22.5° is poor compared with heading 0° case.

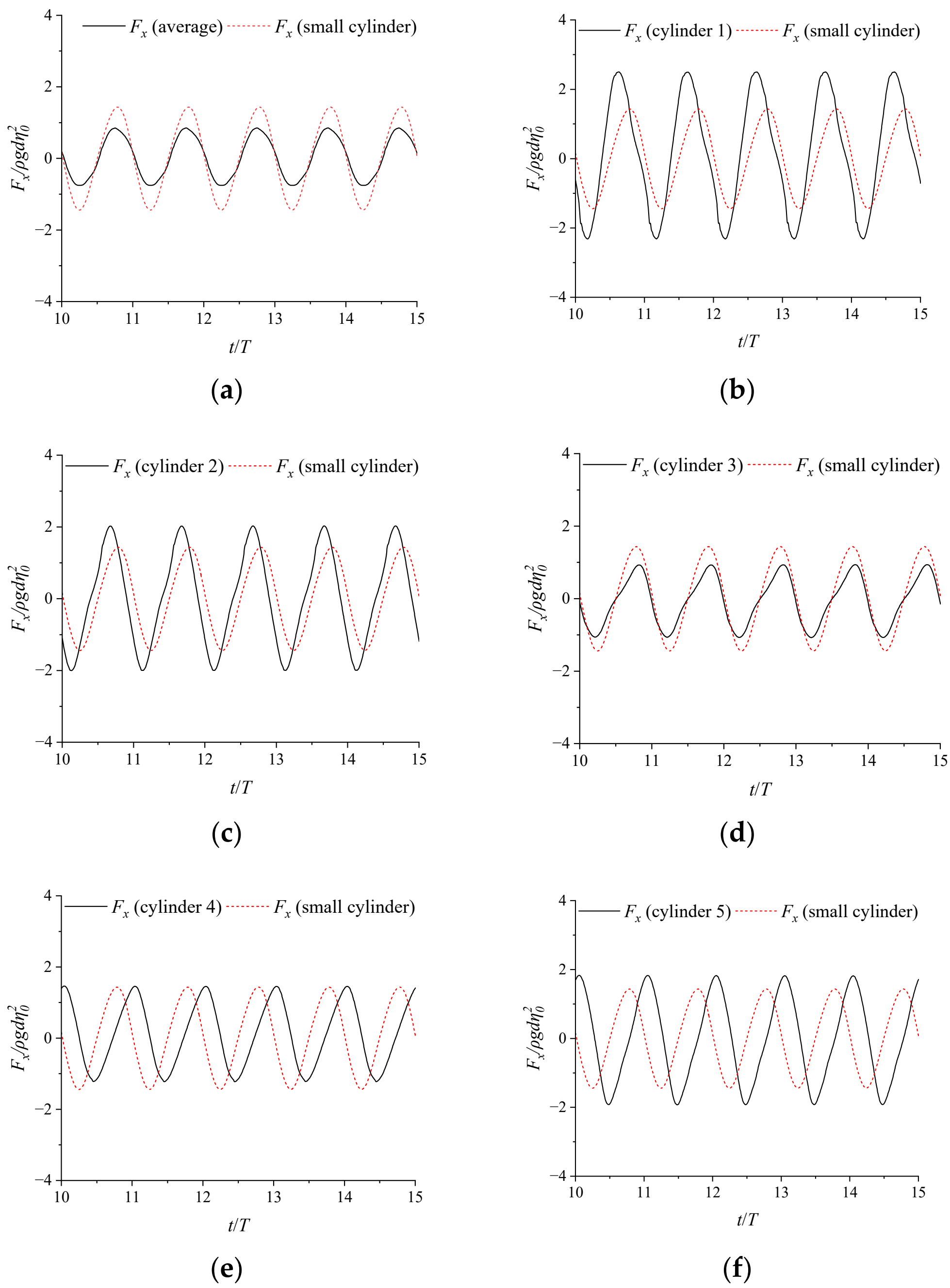

Figure 25. Wave forces on the SPEC: (**a**) average wave force; (**b**) cylinder 1; (**c**) cylinder 2; (**d**) cylinder 3; (**e**) cylinder 4; (**f**) cylinder 5.

4.4. Performance of the SPEC at Different Wave Numbers

The dimensions of the structure are optimized under the target wave number $k_0c = 1.0\ \mathrm{m}^{-1}$, where $c = 3.3448$ is the specific value between the optimized dimensions and the experimental dimensions. According to the research results in Section 4.2, under the interaction with nonlinear waves, the concentrator still shows self-protection performance and concentration effects at $S = 0.04$ to some extent, so four wave numbers $k_0c = 0.6, 0.8, 1, 1.2\ (\mathrm{m}^{-1})$ with a wave steepness of 0.04 are adopted for comparative study. The specific incident wave parameters are presented in Table 7.

Table 7. Wave parameters at different wave numbers.

k_0c (m^{-1})	η_0 (m)	L (m)	T (s)	S
0.6	0.125	3.131	1.4	0.04
0.8	0.094	2.348	1.2	0.04
1	0.075	1.878	1.1	0.04
1.2	0.063	1.565	1	0.04

Figures 26–29 plot the dimensionless wave elevations (η/η_0) outside the concentrator at different wave numbers. To compare the performance, the big single-cylinder (r_b = 0.478 m) and the small single-cylinder (r_s = 0.125 m) are considered in this section. For k_0c = 0.6 m^{-1} and k_0c = 0.8 m^{-1}, the wave elevation of the SPEC is between the results of two single-cylinders. From the results of k_0c = 1.2 m^{-1} case shown in Figure 29, the wave elevation is closer to the value of the big single-cylinder, and the self-protection performance is noneffective on the weather side. In addition, the disturbance of the wave surface outside the concentrator is the largest for the short-wave case (k_0c = 1.2 m^{-1}), which verifies the influence of short wave on the self-protection performance.

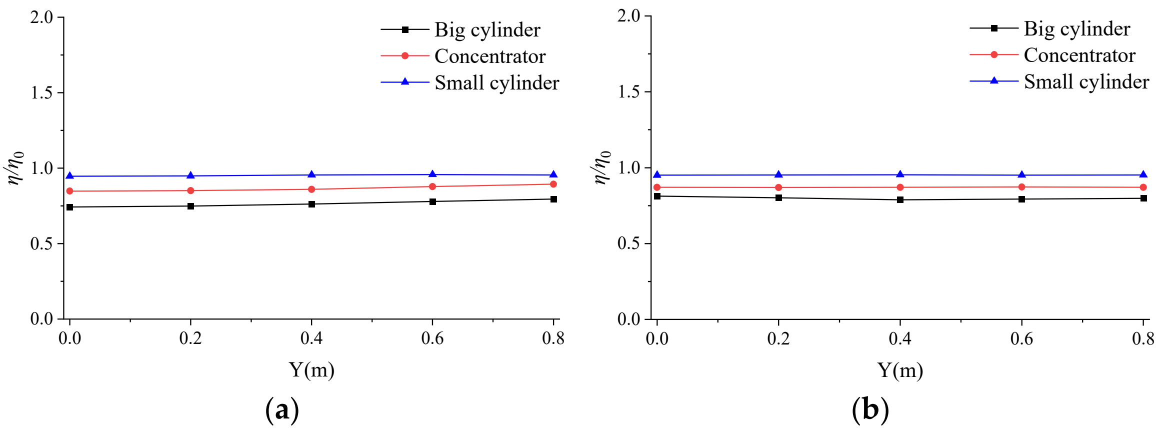

Figure 26. The numerical wave elevation at k_0c = 0.6 m^{-1}: (**a**) Weather side; (**b**) Lee side.

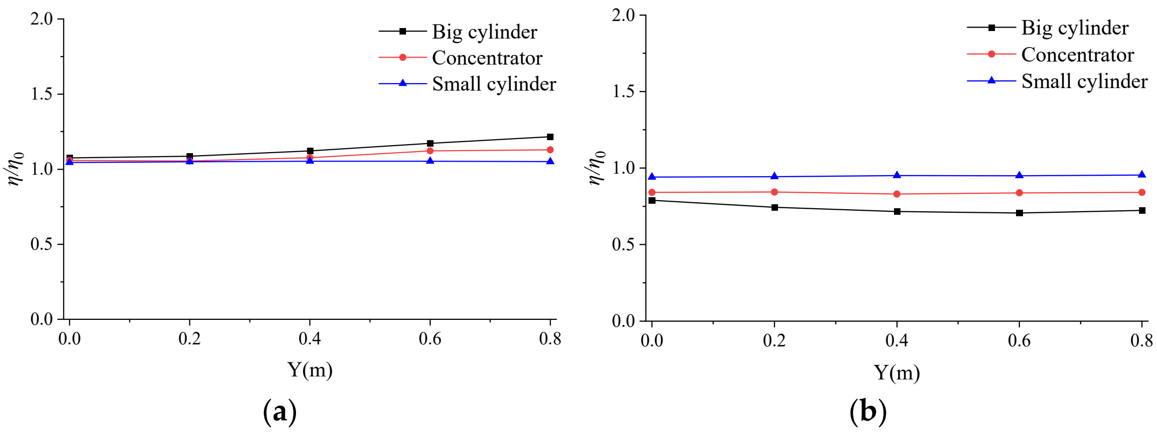

Figure 27. The numerical wave elevation at k_0c = 0.8 m^{-1}: (**a**) Weather side; (**b**) Lee side.

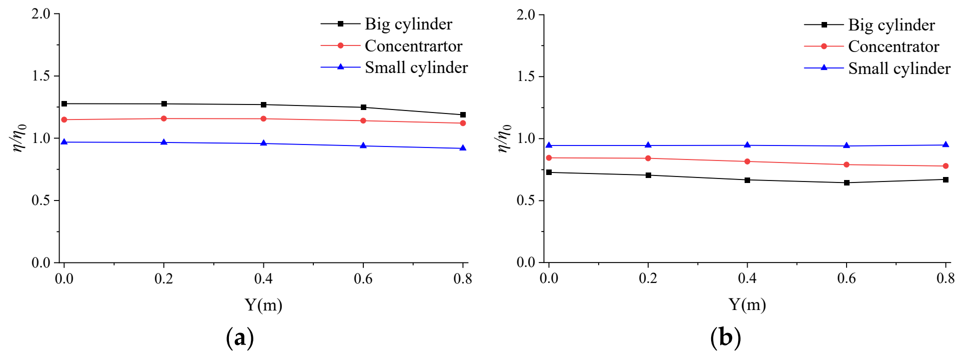

Figure 28. The numerical wave elevation at k_0c = 1.0 m^{-1}: (**a**) Weather side; (**b**) Lee side.

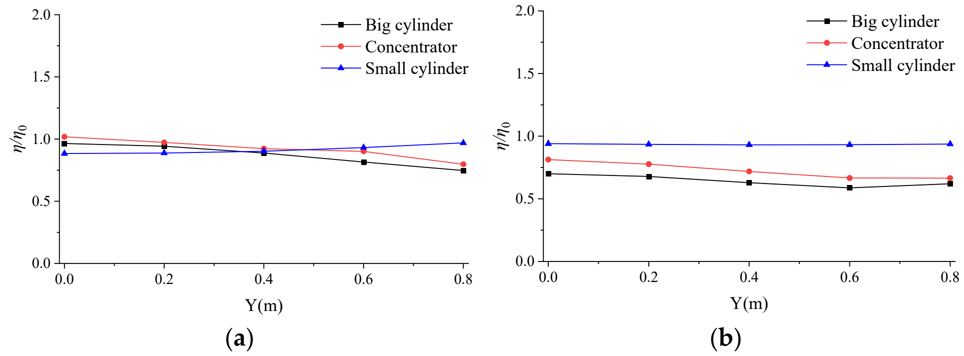

Figure 29. The numerical wave elevation at k_0c = 1.2 m^{-1}: (**a**) Weather side; (**b**) Lee side.

The wave elevation monitored by the central wave probe is plotted in Figure 30. It is obvious that the concentration effects are almost invalid at k_0c = 0.6 m^{-1} and k_0c = 1.2 m^{-1}. Besides, although the value of η/η_0 is still larger than 1 at k_0c = 0.8 m^{-1}, the concentration effects are poorer than those at the target wave number k_0c = 1.0 m^{-1}. It can be concluded that the change of wave number will weaken the self-protection performance, while the short wave has a greater impact on the concentration effects.

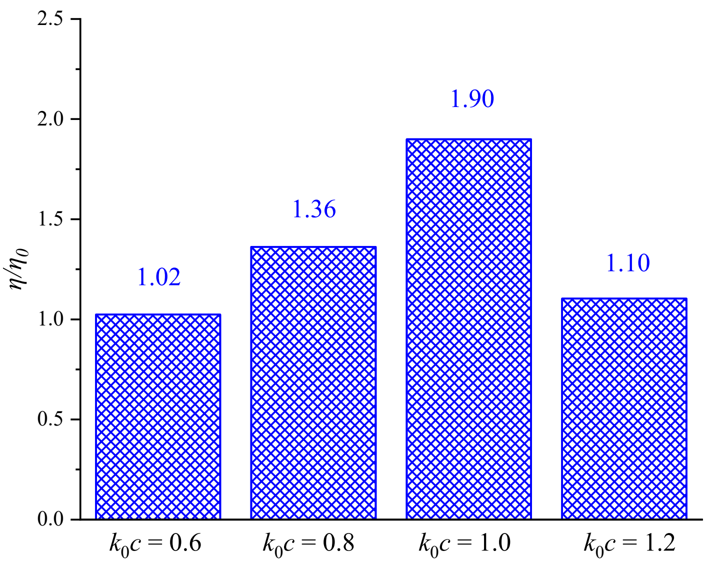

Figure 30. Dimensionless wave elevation (η/η_0) at the center of the SPEC under various wave numbers.

Looking at Figure 31a, the average wave force is almost the same as the wave load of the small single-cylinder at k_0c = 0.6 m^{-1}. The average wave force increases with the increased wave numbers, but the difference between the average wave force and the wave force on the small single-cylinder also increases. The conclusion can be drawn that long wave will reduce the efficiency of overall protection of the SPEC.

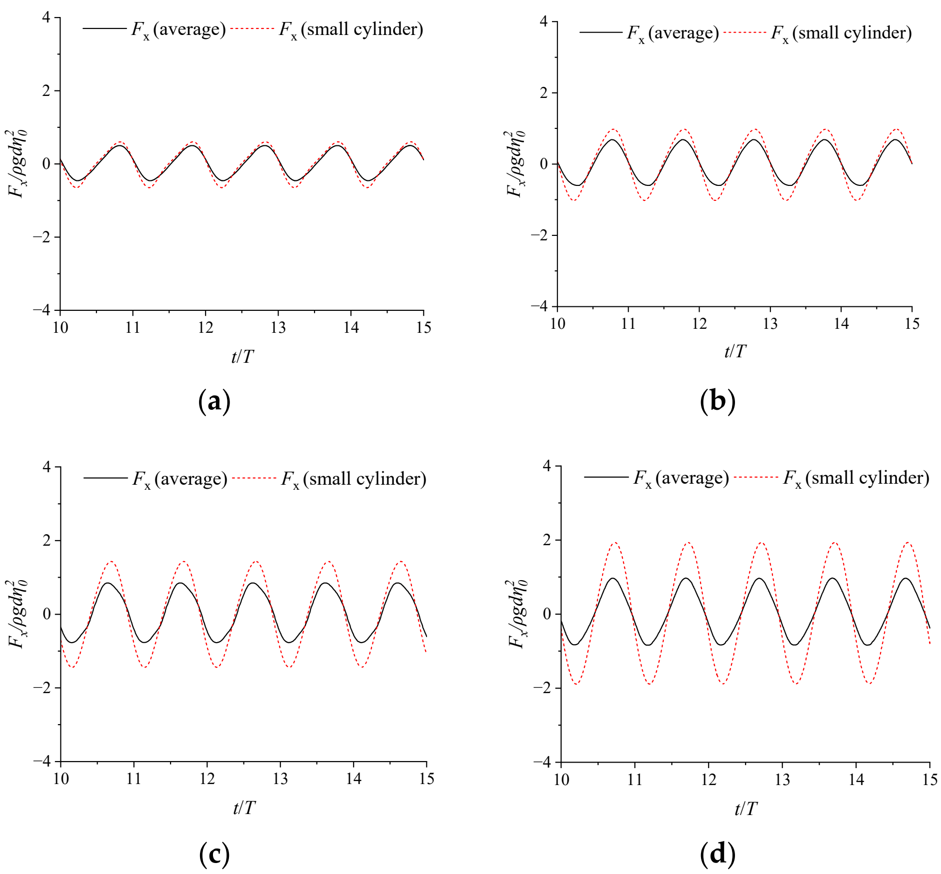

Figure 31. Average wave forces on the SPEC against different wave numbers: (**a**) k_0c = 0.6 m^{-1}; (**b**) k_0c = 0.8 m^{-1}; (**c**) k_0c = 1.0 m^{-1}; (**d**) k_0c = 1.2 m^{-1}.

5. Conclusions

In this paper, a numerical model of two-phase flow was established for hydrodynamic analysis. The self-protection performance and concentration effects of the SPEC were studied under the interaction with nonlinear waves. The numerical validity of the NWT was verified through convergence studies. Then, the wave elevation near the single column and the wave force of the column were simulated, and the results are in good coincidence with the experimental data. In addition, the hydrodynamic analysis of the self-protected energy concentrator (SPEC) was carried out. It is proven that the CFD can simulate the nonlinear wave–object interaction more accurately by comparing with potential flow results and experimental data.

The self-protection performance and concentration effect of the SPEC under various wave-steepness conditions were simulated. The results show that with the increased wave steepness, the wave nonlinearity is enhanced, and the self-protection performance and concentration effects deteriorate. The average wave force on the SPEC under various wave-steepness conditions is smaller than that of the small single-cylinder. It is worth noting that the individual cylinders are more susceptible to the impact of wave force than the whole structure.

Under different wave directions, there is no significant difference in the wave elevation inside and outside the concentrator. The average wave forces at different wave directions are smaller than that of the small single-cylinder, while the concentrator at heading 22.5° are more likely to suffer from local impact than that at heading 0°. It is noted that the changing of the wave number around the target wave number k_0c = 1.0 m^{-1} will weaken the self-protection and concentration effects, while the short wave has a greater impact on the performance.

Author Contributions: Study design by G.H.; data analysis by H.Z.; literature search by T.C. and H.Z.; figures by T.C. and H.Z.; writing by H.Z.; calculation by H.Z.; validation by G.H. and T.C. All authors have read and agreed to the published version of the manuscript.

Funding: This work was supported by the National Natural Science Foundation of China (11502059), the Taishan Scholar Project of Shandong Province (tsqn201909172).

Institutional Review Board Statement: This study was approved by the Institutional Review Board.

Informed Consent Statement: Informed Consent Statement was obtained from all subjects involved in the study.

Data Availability Statement: The data presented in this study are available on request from the corresponding author.

Conflicts of Interest: The authors declare no conflict of interest.

Nomenclature

L	Wave length
η_0	Incident wave elevation
η	Wave elevation
S	Wave steepness
d	Body draft
F	Wave force
k_0c	Wave number
D	Diameter of the cylinder
r, R	Radius of the cylinder
g	Gravity acceleration
Δt	Time step
$\overline{u}_i$	Time-average velocity component in the x_i -coordinate direction
p_i	Pressure component in the x_i-coordinate direction
ρ	Fluid density
ν	Kinematic viscosity
ν_t	Eddy viscosity
α	Volume fraction

References

1. Muetze, A.; Vining, J.G. Ocean Wave Energy Conversion—A Survey. In Proceedings of the Conference Record of the 2006 IEEE Industry Applications Conference Forty-First IAS Annual Meeting, Tampa, FL, USA, 1 January 2006; IEEE: Piscataway, NJ, USA, 2006; pp. 1410–1417.
2. Cruz, J. *Ocean Wave Energy: Current Status and Future Perspectives*; Springer: Berlin/Heidelberg, Germany, 2008.
3. Kanoria, M.; Mandal, B.N. Water wave scattering by a submerged circular-arc-shaped plate. *Fluid Dyn. Res.* **2002**, *31*, 317–331. [CrossRef]
4. Li, C.; Shih, R.; Weng, W. Investigation of Ocean-Wave-Focusing Characteristics Induced by a Submerged Crescent-Shaped Plate for Long-Crested Waves. *Water* **2020**, *12*, 509. [CrossRef]
5. Gayen, R.; Gupta, S. Scattering of surface waves by a pair of asymmetric thin elliptic arc shaped plates with variable permeability. *Eur. J. Mech.—B/Fluids* **2020**, *80*, 122–132. [CrossRef]
6. Murashige, S.; Kinoshita, T. An ideal ocean wave focusing lens and its shape. *Appl. Ocean Res.* **1992**, *14*, 275–290. [CrossRef]
7. Hu, X.; Chan, C.T. Refraction of water waves by periodic cylinder arrays. *Phys. Rev. Lett.* **2005**, *95*, 154501. [CrossRef] [PubMed]
8. Kim, G.; Portela, C.M.; Celli, P.; Palermo, A.; Daraio, C. Poroelastic microlattices for underwater wave focusing. *Extrem. Mech. Lett.* **2021**, *49*, 101499. [CrossRef]
9. Zhang, C.; Ning, D. Hydrodynamic study of a novel breakwater with parabolic openings for wave energy harvest. *Ocean Eng.* **2019**, *182*, 540–551. [CrossRef]
10. Ren, J.; Jin, P.; Liu, Y.; Zang, J. Wave attenuation and focusing by a parabolic arc pontoon breakwater. *Energy* **2021**, *217*, 119405. [CrossRef]

11. Zhou, B.; Zheng, Z.; Jin, P.; Wang, L.; Zang, J. Wave attenuation and focusing performance of parallel twin parabolic arc floating breakwaters. *Energy* **2022**, *260*, 125164. [CrossRef]
12. Mayon, R.; Ning, D.; Zhang, C.; Chen, L.; Wang, R. Wave energy capture by an omnidirectional point sink oscillating water column system. *Appl. Energ* **2021**, *304*, 117795. [CrossRef]
13. Cappello, B.; Ospanova, A.K.; Matekovits, L.; Basharin, A.A. Mantle cloaking due to ideal magnetic dipole scattering. *Sci. Rep.-Uk* **2020**, *10*, 2413. [CrossRef]
14. Kuznetsova, S.; Groby, J.; García-Raffi, L.M.; Romero-García, V. Stealth and equiluminous materials for scattering cancellation and wave diffusion. *Wave Random Complex* **2021**. [CrossRef]
15. Rastgordani, A.; Ghattan Kashani, Z.; Abrishamian, M.S. Theory and algorithm for tunable mantle cloaking through bulk Dirac semimetal metasurfaces around elliptical cylinders. *Optik* **2021**, *232*, 166564. [CrossRef]
16. Porter, R. Cloaking of a cylinder in waves. In Proceedings of the 26th International Workshop on Water Waves and Float Bodies, Athens, Greece, 17–20 April 2011.
17. Newman, J.N. Cloaking a circular cylinder in deep water. In Proceedings of the 28th International Workshop on Water Waves and Float Bodies, L'Isle sur la Sorgue, France, 7–10 April 2013.
18. Newman, J.N. Cloaking a circular cylinder in water waves. *Eur. J. Mech.—B/Fluids* **2014**, *47*, 145–150. [CrossRef]
19. Zhang, Z.; Liu, S.; Luan, Z.; Wang, Z.; He, G.; He, G. Invisibility concentrator for water waves. *Phys. Fluids* **2020**, *32*, 081701. [CrossRef]
20. Zhang, Z.; He, G.; Liu, S.; Kashiwagi, M.; Iida, T.; Luan, Z. Numerical and experimental studies on a self-protected energy concentrator for water waves. *Ocean Eng.* **2023**, *268*, 113312. [CrossRef]
21. Bai, W.; Feng, X.; Taylor, R.E.; Ang, K.K. Fully nonlinear analysis of near-trapping phenomenon around an array of cylinders. *Appl. Ocean Res.* **2014**, *44*, 71–81. [CrossRef]
22. Cong, P.; Gou, Y.; Teng, B.; Zhang, K.; Huang, Y. Model experiments on wave elevation around a four-cylinder structure. *Ocean Eng.* **2015**, *96*, 40–55. [CrossRef]
23. Konispoliatis, D.N.; Chatjigeorgiou, I.K.; Mavrakos, S.A. Near trapped wave phenomena in an array of truncated cylinders in a perpendicular arrangement in front of a vertical breakwater. *Appl. Math. Model.* **2020**, *83*, 497–525. [CrossRef]
24. Cong, P.; Zhao, M.; Teng, B.; Gou, Y.; Liu, Y. Second-order near trapping of water waves by a square array of vertical columns in bi-chromatic seas. *J. Fluid Struct.* **2023**, *121*, 103916. [CrossRef]
25. Lu, L.; Chen, X.B. Dissipation in the gap resonance between two bodies. In Proceedings of the 27th International Workshop on Water Waves and Float Bodies, Copenhagen, Denmark, 22–25 April 2012.
26. Sun, L.; Zang, J.; Chen, L.; Eatock Taylor, R.; Taylor, P.H. Regular waves onto a truncated circular column: A comparison of experiments and simulations. *Appl. Ocean Res.* **2016**, *59*, 650–662. [CrossRef]
27. Mohseni, M.; Esperanca, P.T.; Sphaier, S.H. Numerical study of wave run-up on a fixed and vertical surface-piercing cylinder subjected to regular, non-breaking waves using OpenFOAM. *Appl. Ocean Res.* **2018**, *79*, 228–252. [CrossRef]
28. Chen, W.; Gao, Y.; Wang, L.; Guo, Z.; Wang, B. Numerical simulation of wave run-up on four cylinders in a square configuration. *Appl. Ocean Res.* **2021**, *108*, 102519. [CrossRef]
29. Wang, X.; Qiao, D.; Jin, L.; Yan, J.; Wang, B.; Li, B.; Ou, J. Numerical investigation of wave run-up and load on heaving cylinder subjected to regular waves. *Ocean Eng.* **2023**, *268*, 113415. [CrossRef]
30. Shih, T.H.; Liou, W.W.; Shabbir, A.; Yang, Z.; Zhu, J. A new k-ε eddy viscosity model for high Reynolds number turbulent flows: Model development and validation. *Comput. Fluids* **1995**, *23*, 227–238. [CrossRef]
31. Kim, J.W.; Sullivan, J.O.; Read, A. Ringing Analysis of a Vertical Cylinder by Euler Overlay Method. In Proceedings of the ASME 2012 31st International Conference on Ocean, Offshore and Arctic Engineering, Rio de Janeiro, Brazil, 1–6 July 2012.
32. Luan, Z.; He, G.; Zhang, Z.; Jing, P.; Jin, R.; Geng, B.; Liu, C. Study on the Optimal Wave Energy Absorption Power of a Float in Waves. *J. Mar. Sci. Eng.* **2019**, *7*, 269. [CrossRef]
33. Mo, W.; Irschik, K.; Oumeraci, H.; Liu, P.L.F. A 3D numerical model for computing non-breaking wave forces on slender piles. *J. Eng. Math.* **2007**, *58*, 19–30. [CrossRef]